J. exp. Biol. 138, 413–429 (1988)
Printed in Great Britain © *The Company of Biologists Limited 1988*

BIOMECHANICS OF FROG SWIMMING

II. MECHANICS OF THE LIMB-BEAT CYCLE IN *HYMENOCHIRUS BOETTGERI*

BY JULIANNA M. GAL* AND R. W. BLAKE

Department of Zoology, University of British Columbia, Vancouver, Canada

Accepted 16 March 1988

Summary

The hindlimb kinematics of *Hymenochirus boettgeri* (Tornier) were investigated using high-speed ciné films. The movement pattern was stereotypic, flexion and extension of the metatarsal-phalangeals and feet always lagging behind flexion and extension of the femora and tibiofibulae. The right hindlimb was modelled as a series of linked circular cylinders and a flat plate. A blade-element approach was used to calculate the quasi-steady drag-based and accelerative force components parallel to the direction of motion, based on the hindlimb kinematics of sequence 1 (see preceding paper). Positive thrust is generated primarily during the initial stages of extension (power stroke) because of unsteady (added mass) effects. Negative thrust occurs over the latter half of extension, despite the continued acceleration of the animal. Hindlimb interaction is thought to provide propulsive thrust for the latter half of the extension phase. It is suggested that a jet and/or reflective effect may be involved.

Introduction

Using a blade-element approach, Blake (1979, 1980, 1981, 1986) developed a general model of the mechanics of drag-based propulsion mechanisms. The model has been applied to pectoral fin swimming in angelfish (Blake, 1979, 1980, 1981) and metapodial limb propulsion in the water boatman (Blake, 1986). Fish (1984) applied a simplified version of the model in an analysis of paddling in muskrat. Previous analyses have assumed that the paddling appendage in question can be viewed as a rigid spar. As far as we are aware, there is no detailed analysis of the mechanics of swimming with jointed appendages in aquatic animals in the literature. Calow & Alexander (1973) calculated thrust production by *Rana temporaria* from body velocity changes recorded over a limb-beat cycle. They determined drag from the deceleration of the body during flexion, concluding that

* Present address: Department of Pure and Applied Biology, University of Leeds, Leeds, LS2 9JT, UK.

Key words: frog, swimming biomechanics, hydrodynamic modelling, thrust.

their resistance estimate was probably high, since it took no account of the effect of hindlimb flexion in producing negative thrust.

Here, the mechanics of the beating cycle of the hindlimb of *Hymenochirus boettgeri* is investigated using a blade-element approach. The hindlimbs are modelled as a series of linked, three-dimensional, circular cylinders and a flat plate. Instantaneous quasi-steady drag and inertial forces generated during flexion and extension of the legs are determined. The sum of these forces in the direction of motion is plotted against time. Results are compared with the force inferred from the whole-body kinematics given in the preceding paper (Gal & Blake, 1988), to determine whether the forces considered in the blade-element model are sufficient to explain the observed swimming behaviour of the frog.

Materials and methods

Frame-by-frame whole-body tracings were made from ciné film records corresponding to the four sequences introduced in the preceding paper. The central long axis of the torso and each hindlimb segment (femur, tibiofibula, metatarsal-phalangeal and foot, hereinafter designated fem, tbfb, mtph and foot, respectively) was estimated, and stick figures were drawn (Fig. 1).

A blade-element approach, based on the kinematics of sequence 1 (see figs 4A, 5A in Gal & Blake, 1988), was used to calculate the quasi-steady drag and accelerative forces generated by hindlimbs in flexion and extension. A high degree of symmetry justified considering the right hindlimb only. Limb angular velocities and angular accelerations were determined as follows. The positional angle of

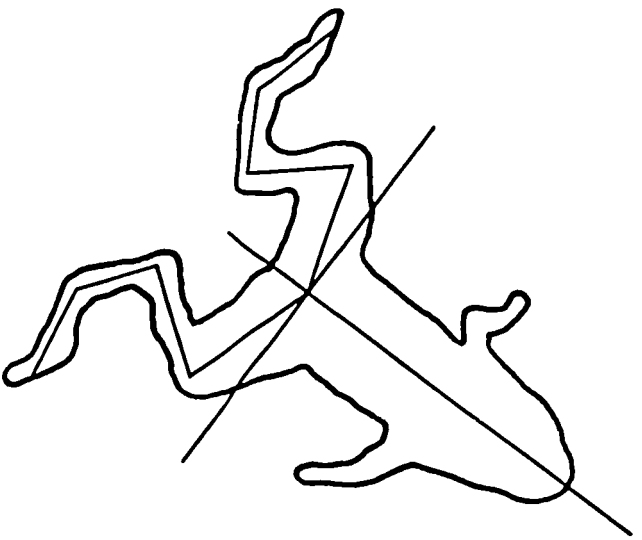

Fig. 1. Frame-by-frame whole-body tracings are made from the ciné film records. The central long axes of the torso and hindlimb segments are estimated, from which stick figures are drawn and positional angles are measured.

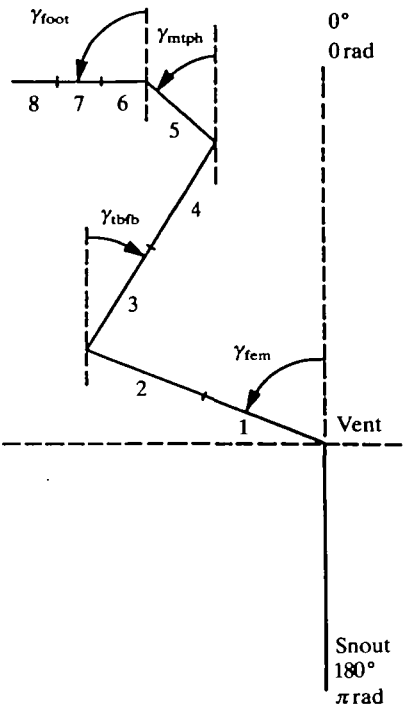

Fig. 2. The positional angles (γ) of the fem, tbfb, mtph and foot segments (of the right hindlimb) are measured with respect to the long axis of the torso. Cranial and caudal rotations of the segments represent increases and decreases in their positional angles, respectively. The segments are further subdivided into elements of similar geometry, numbered 1–8. Element morphometrics are given in Table 1.

each segment of the limb was measured with respect to the long axis of the torso (Fig. 2) and plotted throughout the flexion/extension cycle. These data were smoothed by a seven-point moving polynomial technique (see Gal & Blake, 1988, for a description of the method) to give smoothed angular velocity and angular acceleration for each segment.

Quasi-steady (drag-based) thrust

To calculate quasi-steady resistive forces, the limb segments were further subdivided into eight elements (Fig. 2). Elements of the fem, tbfb and mtph were modelled as three-dimensional circular cylinders. Foot elements were modelled as three-dimensional flat plates. The areas of the elements are given in Table 1, with other blade-element morphometrics. Depending upon the relative velocities of an element and the fluid, the resultant instantaneous drag force could propel or retard the animal. Two-dimensional vector geometry allowed the calculations of relative velocity and associated resistive forces on each element. Fig. 3 illustrates

Table 1. *Hindlimb element morphometrics of sequence 1 animal*

Element number	Element description	Element area (m^2)	Element mass (kg)	Added mass (kg)	Virtual mass (kg)
1	fem (proximal)	$4{\cdot}52\times10^{-6}$			
2	fem (distal)	$4{\cdot}52\times10^{-6}$			
3	tbfb (proximal)	$2{\cdot}30\times10^{-6}$			
4	tbfb (distal)	$2{\cdot}30\times10^{-6}$			
5	mtph	$2{\cdot}38\times10^{-6}$			
6	foot (proximal)	$4{\cdot}17\times10^{-6}$	$1{\cdot}0\times10^{-6}$	$6{\cdot}93\times10^{-6}$	$7{\cdot}93\times10^{-6}$
7	foot (middle)	$1{\cdot}25\times10^{-5}$	$3{\cdot}0\times10^{-6}$	$6{\cdot}14\times10^{-5}$	$6{\cdot}44\times10^{-5}$
8	foot (distal)	$5{\cdot}21\times10^{-6}$	$1{\cdot}25\times10^{-6}$	$3{\cdot}27\times10^{-5}$	$3{\cdot}40\times10^{-5}$

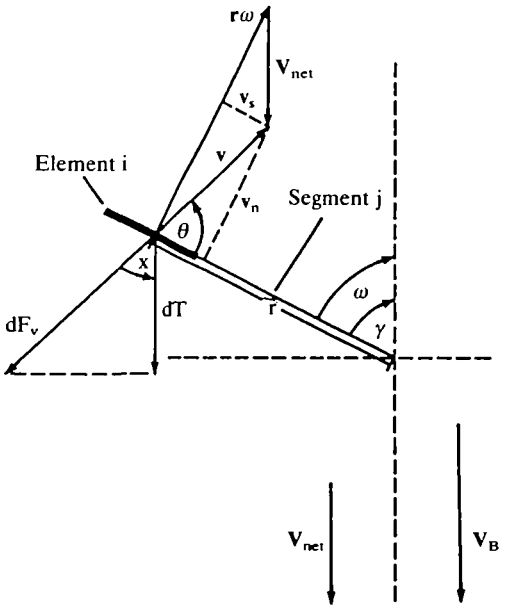

Fig. 3. The drag-based thrust (dT) of element i, located on segment j, is calculated. See text for explanation.

an example of how the component of the drag-based force on an element, parallel to the direction of motion, was calculated.

Consider element i, located at the distal end of segment j. The distance from the midpoint of element i to the pivot point of segment j, is r. The pivot point of segment j has velocity V_{net}. The midpoint of element i has a tangential linear velocity of $r\omega$ (where ω is the angular velocity of segment j). V_{net} opposes $r\omega$, such

that the velocity of element i, relative to the fluid, is v. The magnitude of v is given by:

$$v = \sqrt{(v_n^2 + v_s^2)}\,, \tag{1}$$

where

$$v_n = r\omega + V_{net}\sin\gamma \quad \text{and} \quad v_s = V_{net}\cos\gamma\,, \tag{2}$$

and γ is the positional angle of segment j. The drag force dF_v, opposing the relative velocity v, is given by:

$$dF_v = \tfrac{1}{2}\rho A_p C_D v^2\,, \tag{3}$$

where ρ, A_p and C_D are fluid density, projected area and drag coefficient, respectively. The component of this resistive force parallel to the direction of motion, dT, is equal to:

$$dT = dF_v\cos x\,, \tag{4}$$

where $x = 180°-\gamma°-\theta°$ (π rad$-\gamma$ rad$-\theta$ rad), and θ is the hydrodynamic angle of attack of element i. θ is given by:

$$\theta = \arcsin(v_n/v)\,. \tag{5}$$

The projected areas of the cylindrical elements (fem, tbfb and mtph elements) are given by the product of their length and diameter. The projected areas of the foot elements were measured directly from the ciné film. Film frames immediately preceding sequence 1 showed the animal rotating in the plane of the camera, where the expanded foot could be accurately measured.

The drag coefficients of the foot elements are functions of θ:

$$C_D = 1{\cdot}1 \text{ for } \theta \pm 45° \text{ (0·77 rad) from } 90° \text{ (1·57 rad)}\,, \tag{6}$$

$$C_D = k\sin\theta \text{ for } \theta < 40° \text{ (0·70 rad)}\,, \tag{7}$$

where $k = 2{\cdot}5$ (from Blake, 1979). The drag coefficients of the cylindrical elements are also functions of θ:

$$C_D = 1{\cdot}1\sin^3\theta + 0{\cdot}02 \tag{8}$$

(Hoerner, 1965) for subcritical Reynolds numbers (i.e. $Re < 5{\cdot}0\times10^5$).

For the purpose of this analysis, the direction of the forward velocity of the animal (V_B, 'vent' velocity, see fig. 4A in Gal & Blake, 1988) is always positive. The directions of angular velocities of the hindlimb segments are therefore positive during flexion and negative during extension. A propulsive force is generated by an element only when it is effectively moving backwards (negative relative velocity, v). Because they are linked, proximal segments influence the velocities of distal ones. V_{net} describes the velocity that any segment 'sees' as a result of being attached to other moving parts. It is equal to V_B for the fem segment. For the foot segment, V_{net} is equal to the sum of V_B and all the velocity contributions parallel to the direction of motion of the more proximal segments. V_{net} may be negative or positive for the proximal and distal segments, respectively, during extension. It is always positive for every segment during flexion. Specific vectors were adjusted according to the particular element being con-

sidered. The total drag-based force generated by the right hindlimb, parallel to the direction of motion, is therefore equal to the sum of the dT contributions of all the elements throughout flexion and extension. This value is doubled to give the total for both hindlimbs:

$$dT_{tot} = 2 \sum_{e=1}^{e=8} dF_v \cos x \,. \tag{9}$$

Unsteady (accelerative-based) thrust

The forces associated with the unsteady movement of the legs must be considered. When a body is accelerated through a fluid, a volume of fluid is entrained with it. The force must be sufficient to accelerate the mass of the body and the mass of the volume of fluid entrained (the added mass). This added mass depends on the size, orientation and type of motion that the moving body experiences (translational, rotational etc.). The reaction force (acceleration reaction; Daniel, 1984) associated with accelerating the virtual mass (mass plus added mass) of an element is in a direction opposite to that of the acceleration.

There are undoubtedly unsteady forces associated with all the hindlimb segments; however, only those of the foot elements are considered in this analysis. The foot experiences the highest angular accelerations. Being the most distal segment, it also experiences the greatest translational acceleration as a result of the contributions of the extending proximal segments. The example in Fig. 4 shows how two-dimensional vector geometry is used to solve these accelerative forces.

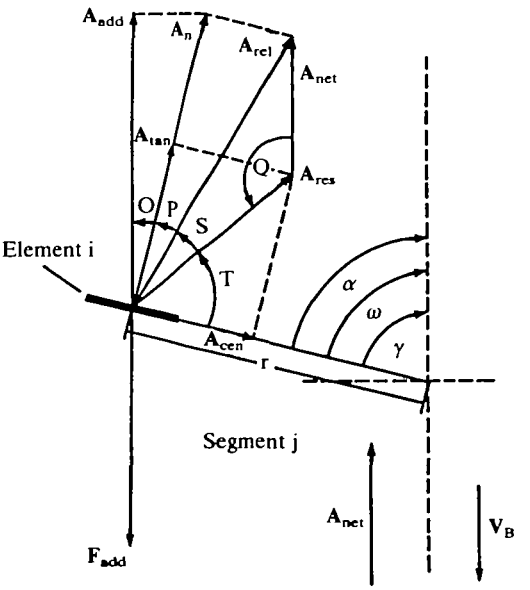

Fig. 4. The accelerative force (F_{add}) of element i, located on segment j, is calculated. See text for explanation.

Consider element i, located at the distal end of segment j. The distance from the midpoint of element i to the pivot point of segment j is r. During extension, segment j has an angular acceleration α, the direction of which opposes the direction of progression of the body (V_B). Element i has a linear tangential acceleration (A_{tan}) of $r\alpha$. Element i also has a centripetal acceleration (A_{cen}) of $(r\omega)^2/r$. The resultant acceleration (A_{res}) of element i is given by:

$$A_{res} = \sqrt{(A_{tan}{}^2 + A_{cen}{}^2)} . \quad (10)$$

Adding A_{net} to A_{res} gives A_{rel}, the relative acceleration of element i to the fluid. A_{net} is analogous to V_{net} as it represents the sum of the acceleration of the body of the animal (vent acceleration of sequence 1, see fig. 5A in Gal & Blake, 1988) and the parallel components of the accelerations of the more proximal segments (mtph, tbfb and fem). A_{rel} is calculated by:

$$A_{rel}{}^2 = A_{net}{}^2 + A_{res}{}^2 - 2A_{net}A_{res}\cos Q , \quad (11)$$

where $Q = \gamma + T$ (γ = positional angle of segment j) and $T = \arcsin(A_{tan}/A_{res})$. The acceleration reaction of element i is proportional to the normal component (A_n) of A_{rel}:

$$A_n = A_{rel}\cos P , \quad (12)$$

where $P = 90° - S° - T°$ ($\frac{\pi}{2}$ rad $-$ S rad $-$ T rad) and $S = \arcsin(A_{net}\sin Q/A_{rel})$. The component of the acceleration reaction parallel to the direction of motion (F_{add}) is proportional to A_{add}:

$$A_{add} = A_n\cos O , \quad (13)$$

where $O = 90° - \gamma$ ($\frac{\pi}{2}$ rad $-\gamma$ rad). F_{add} is therefore given by:

$$F_{add} = m_{virtual}A_{add} , \quad (14)$$

where $m_{virtual}$ is the mass of the element plus its associated added mass. The added masses of the foot elements were generated by solving for the mass of the volume of fluid described by rotating rectangular area-equivalents of each element about the long axis of the foot segment (see Table 1 for virtual masses of the foot elements). Only translational added masses are considered in this analysis; rotational added mass coefficients are omitted. In this example, F_{add} is propulsive (i.e. in the same direction as the velocity of the body, V_B). The total unsteady force generated by the foot during extension alone ($F_{add,tot}$) is the sum of all F_{add} values of each foot element:

$$F_{add,tot} = 2\sum_{e=6}^{e=8} m_{virtual}A_{add} . \quad (15)$$

Results

Symmetrical composite stick diagrams, illustrating the positions of the hindlimb

segments relative to the long axis of the torso, are shown in Fig. 5A,B (during flexion 1–5, and extension 6–10). This stereotypic pattern is characterized by the following five stages, beginning with Fig. 5A1.

(i) Flexion of fems and tbfbs; mtphs and feet maintained parallel to the long axis of the torso.

(ii) Flexion of mtphs and feet; feet folded and webbing collapsed.

(iii) Extension of tbfbs to place feet well beyond the knees.

(iv) Extension of fems and tbfbs; mtphs and feet maintained normal to the long axis of the torso.

(v) Extension and rotation of mtphs and feet.

Flexion and extension of the mtphs and feet always lag behind flexion and extension of the fems and tbfbs.

The positional angles recorded for the right hindlimb segments of sequence 1 are shown in Fig. 6. Flexion is defined as ending at stage ii, before the outward displacement of the feet (stage iii). Extension is defined as beginning at stage iv, after the outward displacement of the feet (stage iii). The positional angles of the fem, mtph and foot increase approximately in phase and reach a maximum at the end of flexion. Tbfb shows an early decrease in positional angle, corresponding to the lateral movement of the feet (stage iii). There is essentially a decrease in positional angle throughout extension in all segments. Mtph and the foot continue to decrease in positional angle, beyond the stages of extension 'proper', because fem and tbfb begin to flex again. The foot shows the most pronounced change in positional angle. Smoothed values parallel experimental ones.

The angular velocity of each segment is shown in Fig. 7. Negative values indicate extension. The foot experiences the greatest angular velocities during both flexion and extension.

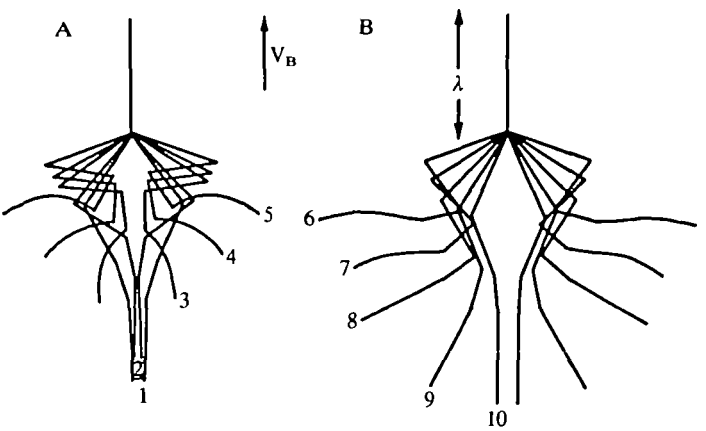

Fig. 5. A symmetrical composite stick diagram of the torso and hindlimb segments of *Hymenochirus boettgeri*. The numbers 1–5 and 6–10 represent sequential orientations throughout flexion and extension, respectively. The snout–vent length, λ, is shown. V_B indicates the body (vent) velocity of the animal.

The angular acceleration of each segment is shown in Fig. 8. Segments accelerating and decelerating during extension will have negative and positive values, respectively. Peak accelerations of the fem, mtph and foot segments are approximately in phase during extension. The foot reaches a maximum angular acceleration of about 1200 rad s^{-2} during the initial stages of the extension phase.

The relative velocities of five of the eight hindlimb elements (elements 2, 4, 5, 6 and 8, see Fig. 2; Table 1), calculated by the method outlined in Fig. 3, are shown in Fig. 9. A negative value reflects a 'backward' movement. Elements 4 and 5 experience a brief negative velocity early in extension. The foot elements 6 and 8 (and element 7, not shown) move backwards throughout the first half of the extension phase. During the latter half of extension, the rearward velocity of these elements is overcome by the forward velocity of the body. Elements 1, 2 and 3 (1 and 3 not shown) never have a rearward velocity great enough to exceed the forward velocity of the body.

The total force generated by both hindlimbs is shown in Fig. 10. The quasi-steady drag component is proportional to the square of the relative velocities of all the right hindlimb elements during flexion and extension (except the foot elements during flexion). The accelerative component is derived from the relative acceler-

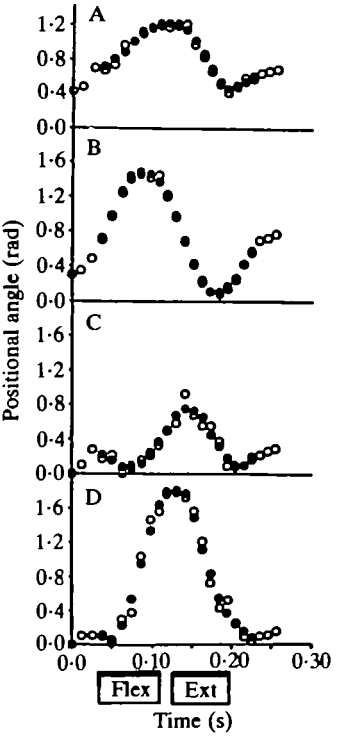

Fig. 6. The experimental (○) and smoothed (●) positional angles of the right hindlimb segments (A, fem; B, tbfb; C, mtph; D, foot) throughout the hindlimb flexion (flex) and extension (ext) (as defined in Results) of the sequence 1 animal.

ations of the right foot elements, but only during extension. Flexion of the hindlimbs generates negative thrust. The positive thrust generated just prior to extension 'proper' is related to the movements corresponding to stage iii, the lateral displacement of the feet. The net positive thrust produced during the first half of the extension phase is almost completely accelerative. The drag-based

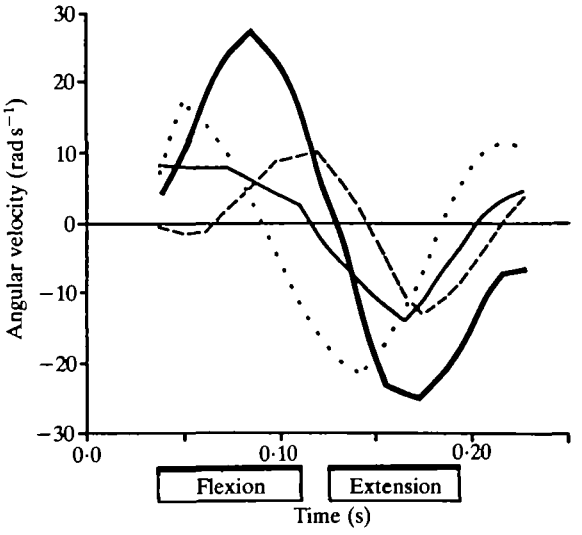

Fig. 7. The smoothed angular velocities of the right hindlimb segments (fem ——, tbfb - - - - -, mtph — — —, foot ——) throughout the hindlimb flexion and extension (as defined in Results) of the sequence 1 animal.

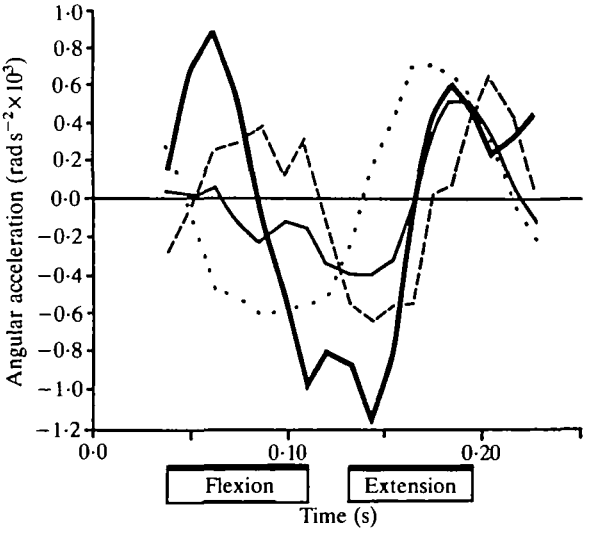

Fig. 8. The smoothed angular accelerations of the right hindlimb segments (fem ——, tbfb - - - - -, mtph — — —, foot ——) throughout the hindlimb flexion and extension (as defined in Results) of the sequence 1 animal.

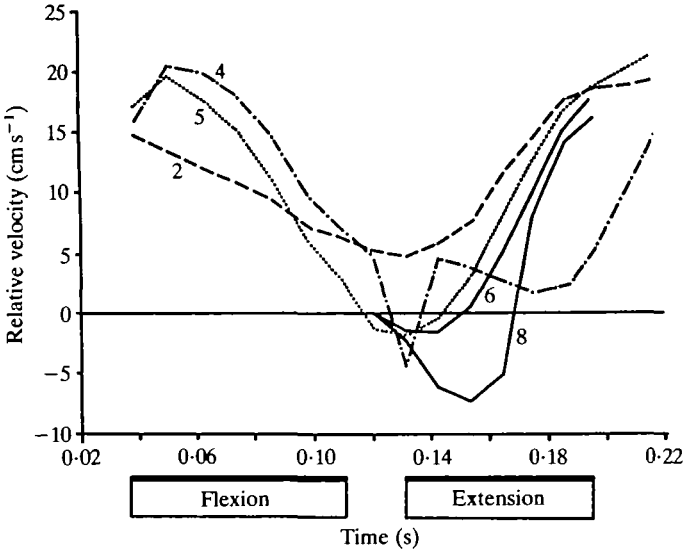

Fig. 9. The relative velocity (v, see Fig. 3) of the right hindlimb elements (2 – – –, 4 – · –, 5 · · · · · ·, 6 ——, 8 ——, see Fig. 2) throughout the hindlimb flexion and extension (as defined in Results) of the sequence 1 animal. A negative relative velocity represents a 'backward' movement of the element.

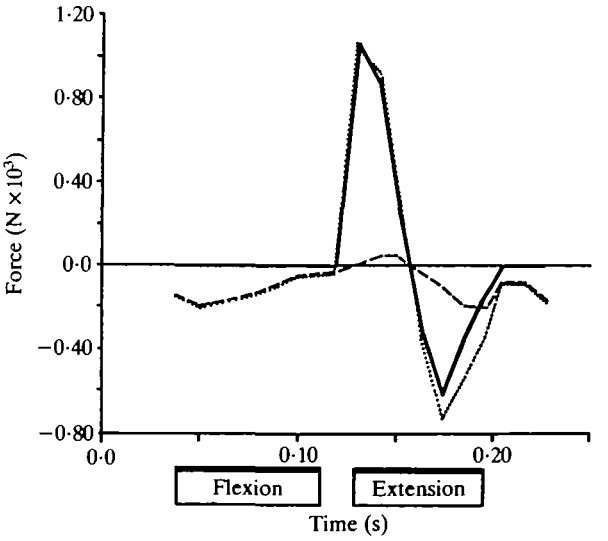

Fig. 10. The total drag-based (dashed line, dT_{tot}) and total accelerative (solid line, $F_{add,tot}$) forces throughout the hindlimb flexion and extension (as defined in Results) of the sequence 1 animal. The dotted line shows the sum of the two force components.

forces generated during this phase are negligible by comparison. At about the midpoint of the extension phase, the forward velocity of the body has overcome the backward velocities of the foot elements, resulting in negative drag-based thrust over the latter half of hindlimb extension. The deceleration of the hindlimb segments during the latter stages of extension contribute to the generation of a substantial negative accelerative impulse, about 2·5 times that of the corresponding negative drag-based impulse.

Discussion

The pattern of movement illustrated in Fig. 5 is stereotypic. During flexion, the mtphs and feet are always drawn up behind the fems and the tbfbs and may be shielded, reducing resistance during hindlimb flexion. Prior to extension proper, the tbfbs are rotated to position the feet laterally beyond the knees. This movement appears to generate some positive thrust (Fig. 10 and see Fig. 11). Lateral placement of the feet may function to increase the mass of undisturbed fluid that is influenced, thereby enhancing the propulsive effort of the animal.

The components of the quasi-steady drag and unsteady forces, parallel to the long axis of the frog's body, have been calculated on the basis of the hindlimb kinematics of sequence 1, a complete flexion/extension cycle. The assumptions involved in this calculation should be considered. Only the right hindlimb kinematics were used directly, and all final force values were doubled to account for the action of both legs. Since sequences were specifically chosen for hindlimb symmetry, this is a valid simplification. The movement of the hindlimbs throughout flexion and extension was coplanar with the long axis of the animal's body, such that two-dimensional vector geometry was sufficient to calculate resultant forces.

The hindlimb was modelled as a series of linked three-dimensional circular cylinders and a flat plate, in free flow (fem, tbfb, mtph and foot, respectively). These were further divided into elements, i.e. smaller units of similar geometry. The elements were assigned drag coefficients corresponding to their technical equivalents. Previous blade-element modelling studies (e.g. Blake, 1979, 1986) have assigned force coefficients to the elements of the swimming appendages (the pectoral fin of the angelfish, the swimming leg of the water boatman), based on the flat-plate analogy. Blake points out that it is likely that only the outermost element experiences anything like 'free flow', but concludes that since this element was responsible for about 90 % of the propulsive thrust, the input from inboard elements was relatively unimportant. Drop-tank experiments with a frog's foot and acetate models thereof (Gal & Blake, 1987) gave drag coefficients similar to those derived from experiments with dynamically similar three-dimensional flat plates, normal to the free flow ($C_D \approx 1{\cdot}1$; Hoerner, 1965). Perhaps more importantly, the 'subtraction method' of Gal & Blake (1987) shows, at least at higher Reynolds numbers (>1000), that the foot behaves like a flat plate in free flow, even when it is attached to the limb ($C_D \approx 1{\cdot}0$). These results justify using

three-dimensional flat plate equivalents to describe the hydrodynamic properties of the frog's foot, and support previous modelling studies involving propulsion by rigid spar-like appendages.

However, the frog's jointed legs introduced a level of complexity not involved in previous studies. Empirical data for the fem, tbfb and mtph, analogous to that obtained for the foot, is lacking. It was necessary to employ values for drag coefficients from the literature. The kinematic pattern observed in swimming frogs suggests that interaction between the segments is likely. Shielding may be important in reducing the resistance to flexion. Throughout this calculation, all segments were treated as though they were functionally isolated. The only interaction considered was the extent to which proximal segment velocities and accelerations affected more distal segments. The calculated drag-based forces, particularly during flexion, are probably overestimates. The accelerative-based force calculations during extension are more speculative. Added mass coefficients, sensitive to shape and size, also depend on the type of motion considered (translational, rotational etc.). The foot experienced both translational (due to the extension of proximal segments) and rotational (about the mtph) motion. Here, the added masses of the foot elements are based on translational motion only. Additionally, this acceleration reaction and its coefficient are derived from ideal flow theory, which admits no vorticity. When vortex formation and shedding occurs, analytical solutions for added mass coefficients are more difficult to derive. Birkhoff (1960) suggests that ideal flow theory is applicable within the first three diameters of travel. The added masses of the foot elements were derived from element volumes of rotation (Blake, 1979) and give reasonable estimates.

Fig. 10 shows that positive (propulsive) forces are generated during stage iii movement (see Results) and only during the first half of the extension phase. The feet are mainly responsible for this by virtue of their large area and relatively high rearward acceleration. The accelerative impulse far exceeds the drag-based impulse during the initial period of extension. The small element areas, coupled with low relative velocities, translates to small drag-based forces. The retarding drag-based forces generated by the proximal elements (see Fig. 2) essentially cancel the propulsive drag-based forces of the foot elements, such that the sum of the drag-based contributions of all the elements during the initial stages of extension is zero. Alternatively, the acceleration of the foot segment is quite high (see Fig. 7), and coupled with large element added masses (see Table 1), the accelerative impulse is substantial. It has been suggested that accelerative-based thrust can be an important component of total thrust, if the stroke axis is asymmetrical. Nachtigall (1960) found that both the stroke angle and the axis of rotation of dytiscid beetles is approximately $2\pi/3$ radians, and suggested that they move their swimming legs in a way that would maximize thrust if the acceleration reaction was a dominant source of thrust. Daniel (1984) showed that paired synchronous limbs can generate a maximum accelerative force if the stroke angle and axis of oscillation is $2\pi/3$ radians. Accelerative thrust production by the related bug *Cenocorixa bifida* (Blake, 1986) accounted for about one-third of the

total thrust produced. Stroke angles and axes of rotation were similar to those of the dytiscid beetles investigated by Nachtigall. Though their absolute magnitudes are often difficult to determine, accelerative-based forces can be important sources of propulsive thrust for animals. It is interesting to note that the acceleration reaction outlined by Daniel (1984) also predicts propulsive thrust from decelerating bodies. The high negative acceleration of the hindlimb (particularly the foot) during flexion (see Fig. 8) represents an acceleration vector with a direction opposite to that of the body. The resultant acceleration reaction would be propulsive. The acceleration reaction of the recovery phase (flexion and stage iii) of the limb-beat cycle was not analysed here, but its potential is recognized.

As the animal begins to accelerate and its velocity increases, the relative 'backward' velocities and accelerations of the hindlimb elements diminish. Additionally, any drag-based or accelerative-based forces that are generated during the final stages of extension are laterally directed and are essentially cancelled out. The result is negative (retarding) thrust, throughout the latter half of hindlimb extension. This force calculation is markedly different from the propulsive thrust (T and $\bar{T}$) predicted from the force balance (see Gal & Blake, 1988; fig. 7). The range of T and the inertial requirement, given the pattern of acceleration observed in sequence 1, are compared with the blade-element force calculation in Fig. 11. Drag-based and accelerative forces can only support the

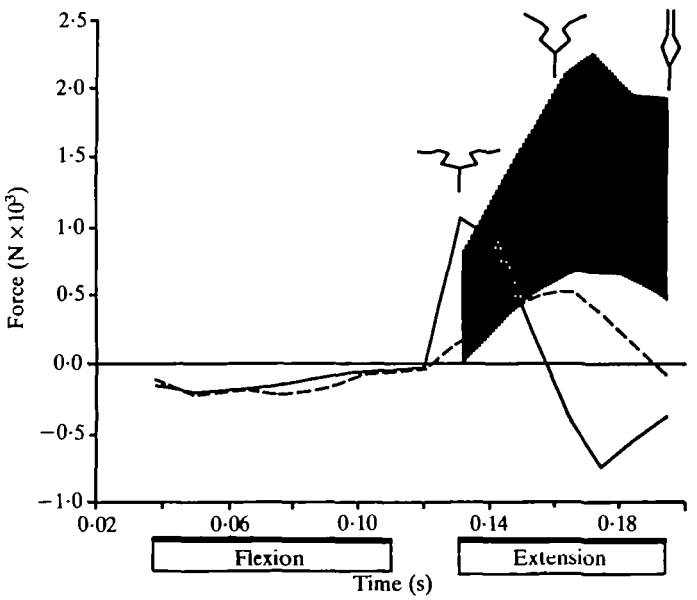

Fig. 11. The total drag-based and accelerative force (—— from Fig. 10) compared to F_{net} (– – – see Gal & Blake, 1988; fig. 7) throughout the hindlimb flexion and extension (as defined in Results) of the sequence 1 animal. The shading indicates the range of T (see Gal & Blake, 1988; fig. 7). The stick figures represent the approximate positions of the hindlimbs at the beginning, midpoint and end of the extension phase.

acceleration of the animal's body during the initial stages of extension. The fact that the animal continues to accelerate, despite corresponding calculations of negative thrust, suggests that an alternative source of propulsive thrust is operating in this system. The transition from positive to negative thrust is concomitant with the hindlimb orientation shown in Fig. 11. Following the extension of the fems and tbfbs, the mtphs and feet begin to extend and rotate towards each other. The force calculation was based on the right hindlimb only, treated as a functionally isolated unit operating in free space, so potential interactive effects between limbs were not considered. It is suggested that an additional force, generated by hindlimb interaction, is responsible for the animal's acceleration during the latter half of the extension phase. Two possible mechanisms come to mind. The first, a 'jet' effect, results from the redirection of the fluid between converging surfaces. This is distinct from jet propulsion involving the contraction of discrete fluid-filled 'sacs' (e.g. medusae and squid). It is likely to be important in aquatic systems where propulsion is achieved by the movement of multiple, closely packed appendages (e.g. errant polychaete worms). The second mechanism, known as a reflective effect, is less well understood. It is known that if two surfaces are brought close together, the total fluid force is greater than the sum of the forces generated by each surface in free flow. It is analogous to the ground effect, where the lift of an aerofoil is enhanced by proximity to a surface (Reid, 1932).

Several observations support the notion of jet and/or reflective effect. The disparity between the calculated and required forces (Fig. 11) occurs when the hindlimbs can physically interact. Hindlimb interaction could not explain such a disparity in the early stages of extension. Of the four sequences previously examined, three showed positive accelerations throughout hindlimb extension (see Gal & Blake, 1988; fig. 5). Gal & Blake (1988; fig. 5B) show that the animal experiences an additional acceleration in a time frame consistent with the interaction and rotation of the mtph and feet. Support for interactive effects also come from observations of *H. boettgeri* during slow swimming. The forelimbs, torso and femoral and tibiofibular hindlimb segments remain quite rigid. The body is propelled only by the rotational movements of the mtphs and feet. In slow swimming, the positional angles of the feet are such that drag-based forces would be poorly directed. However, as the expanded, often bowed, feet rotate, they could squeeze water backwards. Although the sac is less well defined, the combined mobility of the toes and flexible webbing could allow more precise volume and direction control. This would minimize inefficiencies associated with 'leakage'.

The quantitative interpretation of the thrust produced during extension is dependent upon the area of the foot webbing. The rotation of the animal in the plane of the grid, prior to the flexion/extension sequence, allowed an accurate measurement of webbing area (angle subtended by first and fifth phalanges was approximately 120°). It is likely that this measurement may be an underestimate of active swimming area. Additional film sequences, though not suitable for this

analysis, showed the foot webbing to be further expanded (angle subtended by first and fifth phalanges was approximately 160°). This represents an approximate area increase of 33 % (if one considers the foot to be a circular wedge). The drag-based thrust would be proportionately higher, but its contribution to total thrust would still be small. The accelerative thrust is also indirectly dependent on web area, because the added mass coefficients of the foot elements were estimated geometrically from approximations of the volumes of rotation of their rectangular area equivalents. The 33 % increase in web area translates approximately into a 30 % increase in accelerative thrust. Since accelerative thrust is dominant, this is a substantial increase. However, these increases do not change the general interpretation of the results, i.e. that an interactive effect must be taking place. The latter is suggested because of the continued acceleration of the animal throughout extension, despite the apparent 'forward' velocity of the feet at this stage. Inaccuracies in velocity of 10 % should occur in every measurement, such that the relative velocities of the elements and the fluid should not change appreciably. Moreover, abating this directional change would require a two-fold overestimate of body velocity or underestimate of foot velocity (maximum body velocity $\approx 18\,\mathrm{cm\,s^{-1}}$ and maximum rearward foot velocity $\approx 6\,\mathrm{cm\,s^{-1}}$). This is unlikely. Alternatively, one would require a downward current of about $12\,\mathrm{cm\,s^{-1}}$ within the partitions of the test area for the relative difference between the velocities of the foot and the body to be zero. This is also unlikely. Therefore, though the quantitative determination of thrust is probably an underestimate, the interpretation of the system is sound.

It would seem that a combination of reactive, resistive and interactive effects propel the frog. Accelerative forces would seem to be the dominant source of positive thrust over the first half of extension. Interactive forces (probably jet forces), appear to be important in maintaining acceleration of the animal throughout the latter half of extension. The interactive effects are of particular interest, because they suggest the potential for active optimization of fluid propulsion systems by the selection of specific movement patterns or gaits. This idea is supported by the fact that *H. boettgeri* has never been observed to swim by asynchronous hindlimb extension at any speed. Hindlimb asychrony is only associated with directional changes. Although slow swimming in the angelfish is accomplished exclusively by asychronous pectoral fin rowing, water boatmen are always propelled by the synchronous rowing actions of their hind legs (Blake, 1979 and 1986, respectively). Appendage morphology of paddlers tends towards the optimum triangular shape predicted by Blake on theoretical grounds. Although a broad convergence of appendage morphology is evident, paddling animals display considerable variability in appendage movement patterns. Investigating the hydrodynamic consequences of variable stroke patterns would be a worthwhile endeavour.

The force-generating mechanisms addressed here are not mutually exclusive. Within a single locomotor system, several mechanisms may function in concert to produce observed movement patterns. Certainly there are dominant mechanisms,

but categorizing the locomotor behaviour of organisms on this basis could result in the neglect of other important, albeit less obvious, mechanisms.

We would like to thank the Natural Sciences and Engineering Research Council of Canada for financial support. Special thanks are due to Dr J. M. Gosline for his helpful advice on this work.

References

BIRKHOFF, G. (1960). *Hydrodynamics: A Study in Logic, Fact, and Similitude.* Princeton: Princeton University Press.

BLAKE, R. W. (1979). The mechanics of labriform locomotion. I. Labriform locomotion in the angelfish (*Pterophyllum eimekei*): An analysis of the power stroke. *J. exp. Biol.* **82**, 255–271.

BLAKE, R. W. (1980). The mechanics of labriform locomotion. II. An analysis of the recovery stroke and the overall fin beat cycle propulsive efficiency of the angelfish. *J. exp. Biol.* **85**, 337–342.

BLAKE, R. W. (1981). Drag-based mechanisms of propulsion in aquatic vertebrates. In *Vertebrate Locomotion* (ed. M. H. Day), *Symp. Zool. Soc., Lond.* **48**, 29–53. London: Academic Press.

BLAKE, R. W. (1986). Hydrodynamics of swimming in the water boatman, *Cenocorixa bifida*. *Can. J. Zool.* **64**, 1606–1613.

CALOW, L. & ALEXANDER, R. MCN. (1973). A mechanical analysis of the hind leg of a frog (*Rana temporaria*). *J. Zool., Lond.* **171**, 293–321.

DANIEL, T. L. (1984). Unsteady aspects of aquatic locomotion. *Am. Zool.* **24**, 121–134.

FISH, F. E. (1984). Mechanics, power output and efficiency of the swimming muskrat (*Ondatra zibithicus*). *J. exp. Biol.* **110**, 183–201.

GAL, J. M. (1987). Biomechanics of swimming in the frog *Hymenochirus boettgeri*. Masters thesis. University of British Columbia, Vancouver, Canada.

GAL, J. M. & BLAKE, R. W. (1987). Hydrodynamic drag of two frog species: *Hymenochirus boettgeri* and *Rana pipiens*. *Can. J. Zool.* **65**, 1085–1090.

GAL, J. M. & BLAKE, R. W. (1988). Biomechanics of frog swimming. I. Estimation of the propulsive force generated by *Hymenochirus boettgeri*. *J. exp. Biol.* **138**, 399–411.

HOERNER, S. F. (1965). *Fluid Dynamic Drag.* Midland Park, NJ: Published by the author.

NACHTIGALL, W. (1960). Uber Kinematik, Dynamik und Energetic des Schwimmins einheimischer Dytisciden. *Z. vergl. Physiol.* **43**, 48–118.

REID, E. G. (1932). *Applied Wing Theory.* New York: McGraw Hill Book Company.